國 立 交 通 大 學

多媒體工程研究所

碩 士 論 文

多輸入多輸出正交分頻多工系統中頻率域
封包欄位偵測與載波頻率偏移估計之實做

Implementation of Frequency-Domain Boundary Detection and Carrier Frequency Offset Estimation in MIMO-OFDM Systems

研 究 生：謝岳霖

指導教授：陳穎平 教授

中 華 民 國 九 十 八 年 六 月

多輸入多輸出正交分頻多工系統中頻率域封包欄位偵測與載波頻率偏移估計之實做

Implementation of Frequency-Domain Boundary Detection and Carrier Frequency Offset Estimation in MIMO-OFDM Systems

研 究 生：謝岳霖　　Student：Yueh-Lin Hsieh

指導教授：陳穎平　　Advisor：Ying-Ping Chen

國立交通大學

多媒體工程研究所

碩士論文

A Thesis

Submitted to Institute of Multimedia and Engineering

College of Computer Science

National Chiao Tung University

in partial Fulfillment of the Requirements

for the Degree of

Master

in

Computer Science

June 2009

Hsinchu, Taiwan, Republic of China

中 華 民 國 九 十 八 年 六 月

摘要

由於可增進效能與降低正交多頻分工系統上對類比轉數位轉換器的需求，頻率域前端技術變得越來越受人注目。在本篇論文中試著實現兩種頻率域演算法：頻率域上的邊界偵測與頻率域上的載波頻率偏移估算。頻率域上的邊界偵測演算法可在低訊噪比衰退環境中找出正確訊號邊界。爲了解決嚴重的衰退與雜訊，使用了最大相似序列估計的重複序列搜尋。根據模擬的結果，在無循環字首直接序列展頻，單輸入單輸出與多輸入多輸出正交多頻分工系統，帶有 100 ppm 的載波頻率偏移，訊噪比小於或等於 6dB，並在多重路徑的環境下，邊界偵測的錯誤率將會小於百分之一。在實現方法上，若頻率域上的邊界偵測演算法使用了 0.18 微米製程，總共需要二十五萬六千個閘數，供應電壓在 1.2 伏特下需消耗 40.2 毫瓦。因此我們可說此演算法不但可以確保得到足夠的效能，而且也可在頻率域正交多頻分工系統架構下同時支援正交多頻分工系統與非正交多頻分工系統。在另一方面，頻率域上的載波頻率偏移估算演算法是基於加上一個虛擬的載波頻率偏移後所得到的載波頻率偏移新演算法，此演算法適用於存在有 IQ 不平衡效應的情況下並且可以容忍 2dB 的增益錯誤與 20 度的相角錯誤在多重路徑的環境中，此演算法只需要三個連續的訓練序列，並加上額外的頻率偏移藉以減少白色高斯雜訊的影響。模擬的結果顯示出偵測誤差小於傳統載波頻率偏移演算法。在實現方法上，若頻率域上的載波頻率偏移估算演算法使用了 0.18 微米製程，總共需要四萬九千個閘數。

Abstract

Frequency-domain (FD) front-end is an attractive technology to improve performance and to reduce analog-to-digital (A/D) requirements of orthogonal frequency-division multiplexing (OFDM) modems. This thesis tries to implement two algorithms in frequency domain: boundary detection in FD (FD-BD) and carrier frequency estimation in FD (FD-CFO). The FD-BD searches the symbol boundary in low-SNR fading environments. Am iterative sequence search with maximum likelihood sequence estimation (MLSE) is built to resist severe fading and noise. Simulation of non-cyclic prefix (non-CP) direct sequence spread spectrum (DSSS), single-input single-output (SISO) and multiple-input multiple-output (MIMO) OFDM hint the detection errors with a carrier frequency offset (CFO) of 100 ppm and SNR $\leqq$ 6dB are less than 1% in frequency-selective fading. The FD-BD is implemented via 0.18-μm CMOS library, which require 256K gate count and consumes 40.2mW at 1.2V supply voltage. Hence, FD-BD does not only ensure adequate performance, but also make OFDM and non-OFDM frame synchronizations function in FD-OFDM structures. On the other hand, FD-CFO is a novel CFO estimation algorithm, based on pseudo-CFO (P-CFO), to estimate the CFO value under the condition of I/Q mismatch with 2dB gain error and 20-degree phase error in selective fading channel. The FD-CFO requires three training symbols, and rotates training symbols by adding extra frequency offset to reduce the effects of additive white Gaussian noise (AWGN). Simulation results indicate that the estimation error is lower than Moose's algorithm and others. The FD-BD is implemented

via 0.18-μm CMOS library, which requires 49K gate count.

Acknowledgement

This thesis describes research work I performed in the Integration System and Intellectual Property (ISIP) Lab during my graduate studies at National Chiao Tung University (NCTU). This work would not have been possible without the support of many people. I would like to express my most sincere gratitude to all those who have made this possible.

First, I would like to thank my advisor Dr. Terng-Yin Hsu and Dr. Ying-Ping Chen for the advise, guidance, and funding they have provided me with.

Then, I must owe Dr. Sheau-Lin Hsieh a debt of gratitude for the help, although I have been sending my appreciation many times in past 2 years. I can hardly express my gratitude to you for your help. Thanks.

I am very grateful to Shau-Yu Cheng, Ming-Fu Sun, You-Hsien Lin, Wei-Chi Lai, Ta-Young Yuan, and other members of ISIP Lab for their support and suggestions.

Moreover, I appreciate from the heart those guys who always accompany me to resist frustration: Catmeow, Piggy, Charley, and anonymities. And more, Fu-ter, is whom my brother always called my only one friend in NCTU. Thanks for your bless.

Finally, and most importantly, I want to thank my parents, my sisters, brother and Zoe for their unconditional love and support they provide me with. It means a lot to me.

Sincerely, Yueh-Lin Hsieh

June 2009

Table of Contents

List of Figures

List of Tables

Chapter 1

Introduction

OFDM (Orthogonal Frequency Division Multiplexing) is a frequency-division multiplexing scheme utilized as a digital multi-carrier modulation method. Due to its spectrally efficient ability of resisting the multipath fading channel [1], [2], or inter-symbol interference (ISI), OFDM has been adopted by many transmission systems, e.g., WLAN systems based on IEEE802.11 series [3], [4], digital audio broadcasting (DAB) [5], and digital video broadcasting terrestrial TV (DVB-T) [6]. MIMO (Multiple-Input Multiple-Output) OFDM is another technology which makes use of multiple transmitter and multiple receiver antennas to transfer independent data streams simultaneously for increasing diversity and spectral efficiency. The combination of MIMO and OFDM has attracted considerable attention due to its ability to achieve high channel capacity in recent years and is considered as the candidate for next generation wireless communication systems. 802.11n is one of the wireless standards adopted MIMO-OFDM.

Nevertheless, MIMO-OFDM systems are sensitive to imperfect synchronization and non-ideal front-end effect, and caused serious system performance degradation. Boundary detection is an important issue in timing synchronization. Boundary detection refers to the task of finding the precise moment of when individual OFDM symbols start and end. The symbol boundary result defines the DFT window; i.e., the set of samples used to calculate

DFT of each received OFDM symbol. The DFT result is then used to demodulate the subcarriers of the symbol. The performance of the symbol boundary algorithm directly influences the effective multipath tolerance of a OFDM system. An OFDM receiver achieves maximum multipath tolerance when symbol timing is fixed to the first sample of an OFDM symbol. If the boundary detection algorithm can detect the boundary accurately, the DFT window will not contain any samples from other symbols. Hence, the maximum length of the channel impulse response (CIR) that does not cause inter-symbol interference (ISI) is equal to the CP length. This is the maximum possible ISI free multipath length for OFDM system.

One of the key effects is carrier frequency offset (CFO) between transmitter and receiver , which is caused by the effects of Doppler shift of the radio frequency (RF) carrier , the mismatch of local oscillator (LO) between the transmitter and the receiver or phase noise of an oscillator. CFO can introduce inter-carrier interference (ICI) caused by neighbouring carriers that will degrade severely the system performance if without appropriate compensation. On the other hand, I/Q mismatch that coming from non-ideal RF, which is due to the gain and phase mismatch between in-phase (I) and quadrature-phase (Q) paths. More specifically, it occurs when the difference of the phase in I and Q channels from local oscillator is not exactly 90 degree and the gain is not the same. Practically, frequency offset and I/Q mismatch (IQ-M) will jointly occur and degrade the system performance prodigiously.

In the convention, the estimation of CFO and BD are operated in the time domain before FFT. But, the trend of wireless broadband communications had created the need of frequency-domain (FD) front-end receivers [8]-[12] that can relax the analog-to-digital (A/D) requirements and benefit the suppression of narrow band interference (NBI). Additional, the application of OFDM receiver with FD front-end was discussed to provide the potential solution for a multi-standard receiver operating not only at a very wide-band transmissions but also at narrow-band accesses. So, this thesis tries to implement the FD-BD and FD-CFO.

The organization of this thesis is described as follows. The system assumption is presented in Chapter 2. Chapter 3 and Chapter 4 describe the implementation of FD-BD and

FD-CFO individually. Finally, Chapter 5 concludes this thesis and points out the future works.

Chapter 2

System Assumptions

This chapter is going to describe two algorithms in frequency domain in detail: FD-BD and FD-CFO. The FD-BD searches the symbol boundary in low-SNR fading environments. Am iterative sequence search with maximum likelihood sequence estimation (MLSE) is built to resist severe fading and noise. FD-CFO is a novel CFO estimation algorithm, based on pseudo-CFO (P-CFO), to estimate the CFO value under the condition of I/Q mismatch with 2dB gain error and 20-degree phase error in selective fading channel.

Section 2.1 describes the FD-BD algorithm which includes system models, problem statements, and the proposed algorithm of FD-BD. The FD-CFO is introduced in section 2.2 which involves system model and the proposed algorithm of FD-CFO, sequentially.

2.1 FD-BD

2.1.1 System Model

To detect the symbol boundary correctly in frequency-selective fading channel, each packet is assumed to contain several time-domain identical training symbols without any guard interval (GI) for initial synchronizations. The TD training symbols are designed artfully to have good autocorrelation property and bad cross correlation property after delays. The TD training symbols repeat several times in the packet header and each training symbol can be one of two patterns {c,-c}, where $\boldsymbol{c} \triangleq [\boldsymbol{c}_0, \boldsymbol{c}_1, ..., \boldsymbol{c}_{L-1}]^T$ and $[\cdot]^T$ denotes matrix

transposition. Then, the transmitted signal is given by

$$c(t) = [\sum_{i=0}^{L-1} c_i \cdot \Pi(t - nT_s)] * f_T(t) \cdot e^{j2\pi f_c t} \qquad (2.1.1)$$

where $\Pi(t)$ is a function of BPSK modulation and T_s is the symbol period of TD training symbols. $c(t)$ is pass through the transmission filter $f_T(t)$ (shaping filter) to be consistent with the spectrum mask, and up-converted to carrier frequency f_c. The signal $c(t)$ is then transmitted through a multipath frequency-selective fading channel. At the receiver, the signal is first passed through the RF filter and then down converted into baseband signal. After RF down conversion, the received signal of TD training symbol becomes

$$r(t) = \sum_{n}^{N-1} [c(t) * h(t) * f_R(t) \cdot e^{j2\pi \cdot f_{CFO} \cdot t} + w(t)] \cdot \delta[t - nT_s] \qquad (2.1.2)$$

where $w(t)$ represents additive white Gaussian noise (AWGN); $\delta(t)$ is the delta function f_{CFO} is the carrier frequency offset; $h(t)$ is the frequency-selective fading response, and $f_R(t)$ is the lowpass equivalent response of the combined RF and baseband filters in receiver.

The received signal r_t after analog-to-digital converter (ADC) (at 1X sampling rate) and automatic gain control (AGC) can be assumed that $r_t \triangleq [r_t, r_{t+1}, \cdots, r_{t+L-1}]^T$ is a L-dimensional vector of L successive received samples in the training symbol part of a packet. The received signal is expressed as

$$r_t = e^{j2\pi f_{CFO}(tT_s)} \sum_{l=0}^{L_m-1} h_l s_{t-l} + w_t \qquad (2.1.3)$$

where w_t is the complex AWGN; L_m represents the effective channel length; $h \triangleq [h_0, h_1, \cdots, h_{L_m}]^T$ is a vector containing Ts-spaced samples of the channel response; s_{t-l} is the $(t-1)^{th}$ element in training sequence which is one of set $\{c_0, c_1, \cdots, c_{L-1}\}$. Finally, the frequency response of r_t can be expressed as

$$R_t = FFT\left([r_t, r_{t+1}, \cdots, r_{t+L-1}]^T\right) \qquad (2.1.4)$$

where $FFT(\cdot)$ denotes L-point FFT operation.

2.1.2 Problem Statement

When data are transmitted with the channel impairments, e.g. multipath fading and CFO effect, the frame synchronization is essential for packet-based communication systems to figure out the correct symbol boundary. The correlation-based methods are developed with the advantage of easy implementation in receivers, while higher performances can achieve through the methods of [8] and [9], which jointly estimate the channel order and establish the frame synchronization. Even though most of these methods perform pretty well at certain SNR regions, e.g. High SNRs (SNR $\geqq$ 10 dB), it is still important to provide enough reliability for robust packet accesses at lows SNRs.

FD-OFDM receiver, which handles all process in frequency domain, is a potential solution for a multi-standard receiver. Employing the TD preambles in time-domain approaches or FD preambles in frequency-domain analysis, many methods based on repeated preamble structure are hard to be efficiently integrated into the FD-OFDM structures where the frame synchronization needs to process with the TD preambles in frequency domain. To acquire the FD-OFDM receiver can function reliably with different standard at different SNRs, this work is not only to perform a robust FD frame synchronizer in low SNR and severe fading, but also to support OFDM and non-OFDM frame synchronizations via FD-OFDM modems.

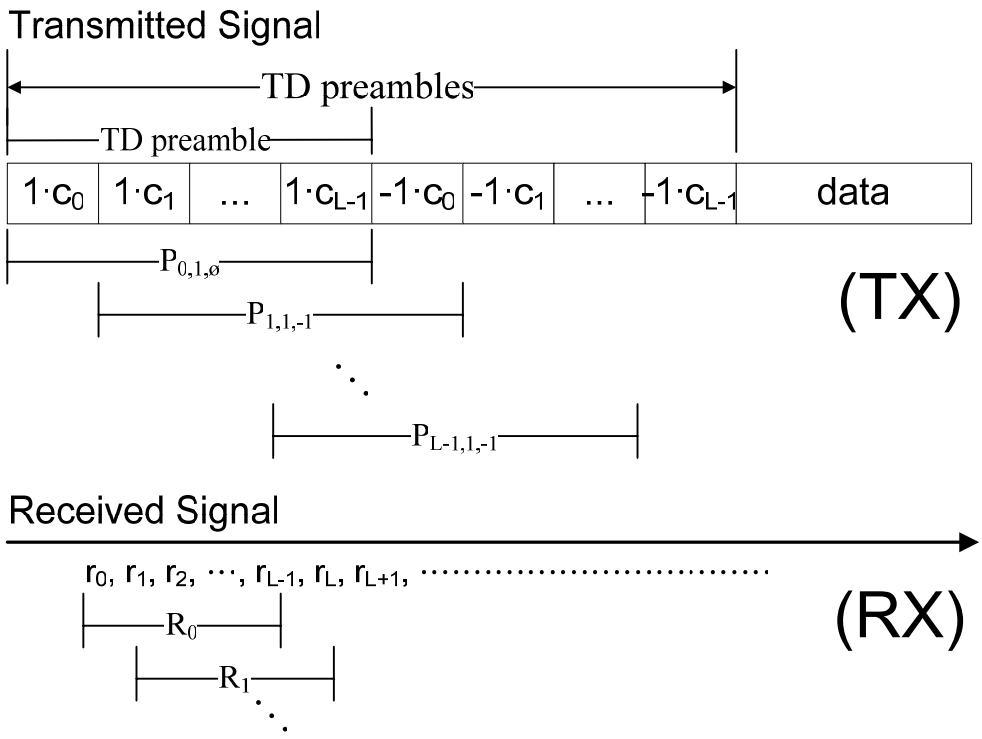

Figure 2-1 Definitions of packet structure with TD preambles in TX and search sequence in RX; in this case, i=1, j=-1, $P_{(0,1,\varnothing)}$ is the frequency response of complete TD preamble (+c), and $P_{(1,1,-1)}$ to $P_{(L-1,1,-1)}$ are the frequency responses of the chip segments cross over two TD preambles (+c -c);

2.1.3 The Proposed Algorithm of FD-BD

Assume the transmitted signals including a sequence of TD preamble signals with length (L+K), which is denoted as $\left\{i\cdot c_{\lambda},\cdots,i\cdot c_{L-1},j\cdot c_{(L)_L},\cdots,j\cdot c_{(\lambda+L+K-1)_L}\right\}$. Both i and j could be ±1 and $0\le\lambda\le L-1$. With the (L+K) consecutive samples $\left\{r_t,r_{t+1},\cdots,r_{(t+L+K-1)}\right\}$, the MLSE [13] makes a decision in favour of the sequence $\left\{i\cdot c_{\lambda},\cdots,i\cdot c_{L-1},j\cdot c_{(L)_L},\cdots,j\cdot c_{(\lambda+L+K-1)_L}\right\}$ to maximize the log joint conditional probability density function (PDF) of $\ln\left[p\left(r_t,r_{t+1},\cdots,r_{(t+L+K-1)}\,|\,i\cdot c_{\lambda},\cdots,i\cdot c_{L-1},j\cdot c_{(L)_L},\cdots,j\cdot c_{(\lambda+L+K-1)_L}\right)\right]$. As shown in Figure 2-1, $\left\{r_t,r_{t+1},\cdots,r_{(t+L+K-1)}\right\}$ can be segmented and transferred to K vectors from r_{t+j} to R_{t+j} with one-to-one mapping via Equation (2.1.4). Thus, the log PDF can be rewritten as $\ln[p(R_t,R_{t+1},\cdots,R_{(t+L+K-1)}\,|\,i\cdot c_{\lambda},\cdots,i\cdot c_{L-1},j\cdot c_{(L)_L},\cdots,j\cdot c_{(\lambda+L+K-1)_L})]$. Because the noise term

in each received signal is independent and R_t only depends on the most recent L transmitted signals, the log PDF can be decomposed as

$$\begin{aligned}&\ln\left[p\left(\boldsymbol{R}_t,\boldsymbol{R}_{t+1},\cdots,\boldsymbol{R}_{t+K-1}\,|\,i\cdot c_\lambda,\cdots,i\cdot c_{L-1},j\cdot c_{(L)_L},\cdots,j\cdot c_{(\lambda+L+K-1)_L}\right)\right]\\&=\ln\left[p\left(\boldsymbol{R}_t\,|\,i\cdot c_\lambda,\cdots,i\cdot c_{L-1},j\cdot c_{(L)_L},\cdots,j\cdot c_{(\lambda+L-1)_L}\right)\right]\\&+\ln\left[p\begin{pmatrix}\boldsymbol{R}_{t+1},\cdots,\boldsymbol{R}_{t+K-1}\,|\,i\cdot c_{(\lambda+1)_L},\cdots,i\cdot c_{(L-1)_L},\\j\cdot c_{(L)_L},\cdots,j\cdot c_{(\lambda+L+K-1)_L}\end{pmatrix}\right]\end{aligned}\qquad(2.1.5)$$

To iterative search the solution of MLSE in Equation (2.1.5), the branch metric of ML rule for each iteration is derived as

$$\Phi\left(R_t,P_{(\lambda,j)}\right)\triangleq\left|(R_t)^H\cdot P_{(\lambda,j)}\right|\qquad(2.1.6)$$

where $\boldsymbol{P}_{(\lambda,j)}\triangleq FFT\left(\left[c_\lambda,\cdots,c_{L-1},j\cdot c_{(L)_L},\cdots,j\cdot c_{(\lambda+L-1)_L}\right]^T\right)$, $P_{(0,\varnothing)}\triangleq FFT\left(\left[c_0,\cdots,c_{L-1}\right]^T\right)$, and $(\cdot)^H$ denotes the conjugate transpose. The iterative sequence search includes a set of search states denoted as $\left\{u_{(0,\varnothing)}\right\}\cup\left\{u_{(\lambda,j)}\right\}_{\substack{1\le\lambda\le L-1\\ j=\pm1}}$, and the rules of allowable state transition defined as

$$\begin{aligned}&u_{(L\text{-}1,\text{-}1)}:P_{(L\text{-}1,\text{-}1)}\to u_{(0,\varnothing)},\qquad u_{(L\text{-}1,1)}:P_{(L\text{-}1,1)}\to u_{(0,\varnothing)},\\&u_{(0,\varnothing)}:P_{(0,\varnothing)}\to\left\{u_{(1,1)},u_{(1,-1)}\right\},\quad u_{(\lambda,j)}:P_{(\lambda,j)}\to u_{(\lambda+1,j)},\end{aligned}$$

where $1\le\lambda\le L-2$. For a complete search with an allowable sequence of length K, L•K state transitions are required. To decrease the number of state transitions and increase the correctness of MLSE estimation, the concept of likelihood confidence and pattern similarity are introduced, which lets the state transition rules become stricter as

$$\begin{aligned}&u_{(\lambda_1,j_1)}:P_{(\lambda_1,j_1)}\to u_{(\lambda_2,j_2)}\\&\quad iff\ \left(\Phi\left(R_t,P_{(\lambda_1,j_1)}\right)\ge\Phi\left(R_t,P_{(\bar{\lambda},\bar{j})}\right)\right)\\&\qquad\wedge\left(conf\left(R_t,P_{(\lambda_1,j_1)}\right)=1\right)\wedge\left(conf\left(R_{t+1},P_{(\lambda_2,j_2)}\right)=1\right)\end{aligned}\qquad(2.1.7)$$

where $\Phi\left(R_t,P_{(\bar{\lambda},\bar{j})}\right)$ is the metric value of Z^{th} ranking similarity, and $conf(R_t,u_{(\lambda,j)})\in\{0,1\}$ is a bit indication of likelihood confidence between R_t and $P_{(\lambda,j)}$. With giving the initial state $u_{\lambda,j}$ at sampling time t and applying the allowable state

transition rule in Equation (2.1.7), the survivor paths $\{\rho_\lambda^k\}$ with K history length can be expressed as

$$\rho_\lambda^k \triangleq u_{(\lambda,j)} : P_{((\lambda)_L,j)},\cdots,P_{((\lambda+K-1)_L,j)} \tag{2.1.8}$$

According to Equation (2.1.5), the survivor metric of each path $\left(\Psi\left(\rho_\lambda^K\right)\right)$ is obtained via the recursive form as follows.

$$\Psi\left(\rho_\lambda^K\right) = \Phi(R_t, P_{(\lambda,j)}) + \Psi\left(\rho_{(\lambda+1)_L}^{K-1}\right) \tag{2.1.9}$$

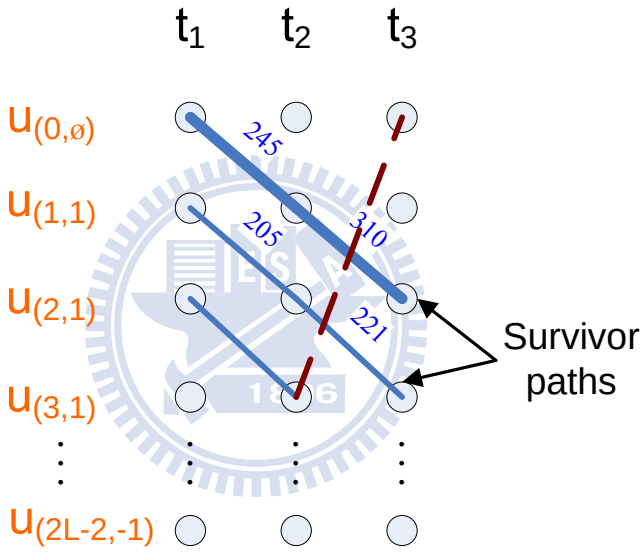

Figure 2-2 Example of trellis diagram

Based on MLSE, the survivor path that contains the maximum metric value is the best option in the set of $\{\rho_\lambda^k\}$. Figure 2-2 employs a trellis diagram to clearly illustrate an example of the proposed iterative sequence searching with Z=4, K=3 and L=16. The dash lines are some cases for unallowable transitions (e.g. $u_{(2,1)} \to u_{(3,1)}$ and $u_{(3,1)} \to u_{(3,1)}$ are not allowable from t_1 to t_2 because of $conf\left(R_{t_1}, P_{(2,1)}\right) = 0$ and $\lambda_{t1} = \lambda_{t2} = 4$, respectively; $u_{(0,\varnothing)} \to u_{(1,1)}$ are not allowable from t_2 to t_3 because of $\Phi\left(R_{t_2}, P_{(0,\varnothing)}\right) < th_2$. Assume the

trellis from t_1 to t_3 containing two survivor paths which are $\rho_0^3 = u_{(0,\varnothing)} : P_{(0,\varnothing)}, P_{(1,1)}, P_{(2,1)}$ and $\rho_1^3 = u_{(1,1)} : P_{(1,1)}, P_{(2,1)}, P_{(3,1)}$. In Figure 2-2 with the case of $\Phi\left(R_{t_1}, P_{(0,\varnothing)}\right) = 210$, $\Phi\left(R_{t_2}, P_{(1,1)}\right) = 245$, $\Phi\left(R_{t_3}, P_{(2,1)}\right) = 310$, $\Phi\left(R_{t_1}, P_{(1,1)}\right) = 220$, $\Phi\left(R_{t_2}, P_{(2,1)}\right) = 205$ and $\Phi\left(R_{t_3}, P_{(3,1)}\right) = 221$, the best survivor path is ρ_0^3 because of $\Psi\left(\rho_1^3\right) = 646$ (220+205+221) and $\Psi\left(\rho_0^3\right) = 765$ (210+245+310). Finally, the iterative sequence search could be repeated M times to obtain more accurate estimation.

Figure 2-3 displays the block diagram of the FD-BD. The FFT sliding window slides over the received samples one-by-one transfer L received samples (in the window) into frequency domain via FFT module. After FFT, the frequency response (Rt) then feeds into the metric computation, which calculates the correlation results between Rt and each pattern (frequency response of ideal TD preamble with different delays) pre-stored in the lookup table (LUT). The correlation results are sorted and recorded in buffers. Then, the iterative sequence search determines the survivor path after collecting sequences of K likelihood estimations. Finally, boundary detection module outputs the decision of timing offset.

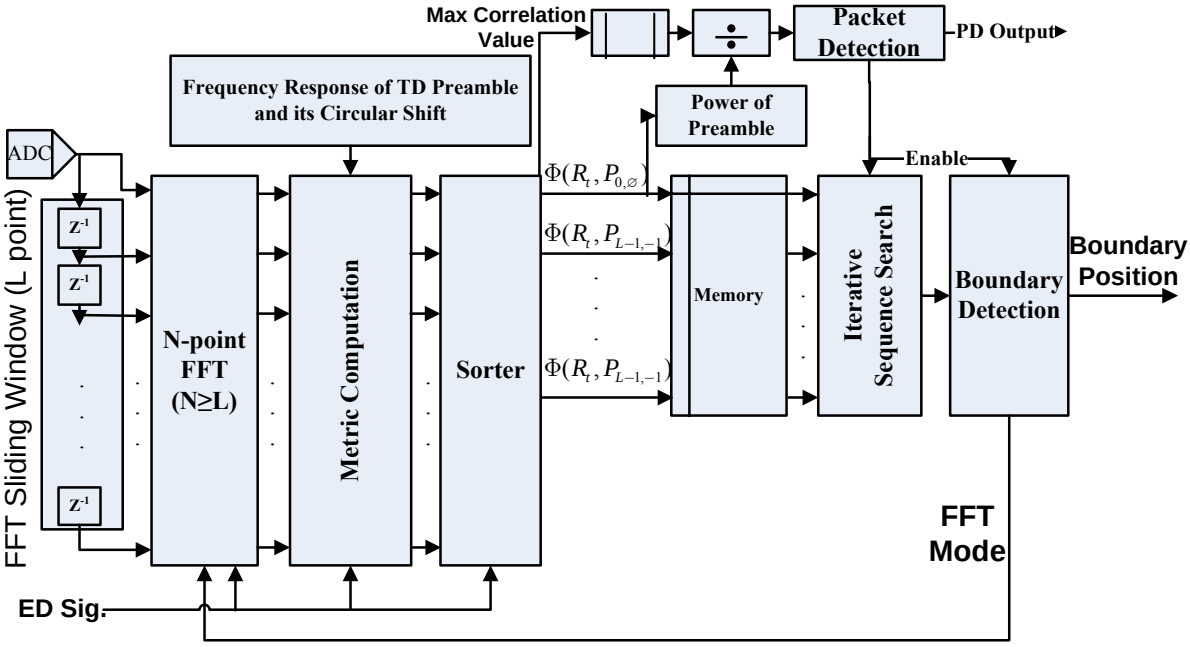

Figure 2-3 Block diagram of FD-BD

2.2 FD-CFO

2.2.1 System Model

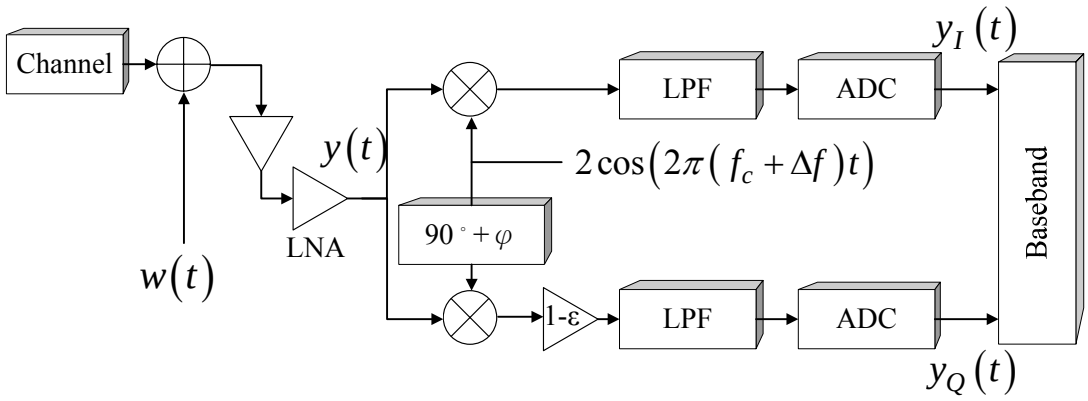

Figure 2-4 Block diagram of receiver's structure

Figure 2-4 schematically depicts a block diagram of a typical OFDM receiver in the presence of CFO and IQ-M. Based on the direct conversion architecture in [8], [19] and [22], the received signal after baseband processing with CFO and IQ-M is given by

$$\begin{aligned} r(t) &= \cos(2\pi\Delta ft)\,\mathrm{Re}\{y(t)\} - \sin(2\pi\Delta ft)\,\mathrm{Im}\{y(t)\} \\ &\quad + j(1-\varepsilon)\begin{Bmatrix}\sin(2\pi\Delta ft-\varphi)\,\mathrm{Re}\{y(t)\} \\ +\cos(2\pi\Delta ft-\varphi)\,\mathrm{Im}\{y(t)\}\end{Bmatrix} + w(t) \end{aligned} \tag{2.2.1}$$

where $y(t)$ and $w(t)$ denote the representations of the received signal in the receiver, and additive white Gaussian noise (AWGN), respectively and ε and φ represent the gain error and phase error introduced from the front-end, respectively. The discrete-time representation of (2.2.1) after the received signal is digitized can be expressed as

$$\begin{aligned} r(t) &= \cos(2\pi\Delta fnT_s)\,\mathrm{Re}\{y(n)\} - \sin(2\pi\Delta fnT_s)\,\mathrm{Im}\{y(n)\} \\ &\quad + j(1-\varepsilon)\begin{Bmatrix}\sin(2\pi\Delta fnT_s-\varphi)\,\mathrm{Re}\{y(n)\} \\ +\cos(2\pi\Delta fnT_s-\varphi)\,\mathrm{Im}\{y(n)\}\end{Bmatrix} + w(n) \end{aligned} \tag{2.2.2}$$

where T_s denotes the sampling period. Furthermore, (2.2.2) can be summarized as

$$r(n) = \xi\cdot y(n)\cdot e^{j(2\pi\Delta fnT_s)} + \sigma\cdot\left(y(n)\cdot e^{j(2\pi\Delta fnT_s)}\right)^* + w(n) \tag{2.2.3}$$

where $(\cdot)^*$ denotes the complex conjugate operation. The received signal can thus be regarded as a gain, denoted by the signal gain (SG) ξ, from the original signal added to the conjugate multiplied by a delta value, called the mirror gain (MG) σ. The signal and mirror gains are represented as follows.

$$\begin{aligned} SG: \xi &= 0.5\left(1+\left(1-\varepsilon\right)e^{-j\varphi}\right) \\ MG: \sigma &= 0.5\left(1-\left(1-\varepsilon\right)e^{j\varphi}\right) \end{aligned} \tag{2.2.4}$$

If neither gain nor phase error exist, then SG remains at unity, and MG decreases to zero. Significantly, the phase rotation is inversed in the direction between the original signals and its conjugate if the CFO is present. Hence, the conventional compensation algorithm, which simply multiplies the data by an exponential term, must be modified in accordance with the gain and phase errors. This work mainly focuses on extracting the CFO value with the IQ-M error.

2.2.2 The Proposed Algorithm of FD-CFO

The FD-CFO adopts three frequency responses of identical training symbols for frequency offset estimation. First, $r(n)_{iq}$, $r(n+N_s)_{iq}$ and $r(n+2N_s)_{iq}$ are defined as three consecutive short preambles, which are distorted by CFO and IQ-M. Then, the short preambles are transform to FD by FFT. The original frequency offset and the pseudo-frequency offset are assumed to be positive in the following mathematical derivations. The three preambles are then rotated by the pseudo-frequency offset.

$$R_1 = FFT\left(\xi y e^{j(2\pi\Delta f n T_s)} + \sigma y^* e^{-j(2\pi\Delta f n T_s)}\right) e^{j(2\pi\Delta\theta n T_s)} \tag{2.2.5}$$

$$R_2 = FFT\left(\xi y e^{j(2\pi\Delta f (n+N_s) T_s)} + \sigma y^* e^{-j(2\pi\Delta f (n+N_s) T_s)}\right) e^{j(2\pi\Delta\theta (n+N_s) T_s)} \tag{2.2.6}$$

$$R_3 = FFT\left(\xi y e^{j(2\pi\Delta f (n+2N_s) T_s)} + \sigma y^* e^{-j(2\pi\Delta f (n+2N_s) T_s)}\right) e^{j(2\pi\Delta\theta (n+2N_s) T_s)} \tag{2.2.7}$$

where $\Delta\theta$ denotes the pseudo-frequency offset. The extra P-CFO is used to resolve the

transformation error resulting from AWGN. Finally,

$$\begin{aligned}
&\frac{\mathrm{Im}\{R_3\}\mathrm{Re}\{R_1\}-\mathrm{Im}\{R_1\}\mathrm{Re}\{R_3\}}{2\left(\mathrm{Im}\{R_2\}\mathrm{Re}\{R_1\}-\mathrm{Im}\{R_1\}\mathrm{Re}\{R_2\}\right)}\\
&=\frac{\sin\left(4\pi\Delta f N_s T_s\right)\cos\left(4\pi\Delta\theta N_s T_s\right)}{2\sin\left(2\pi\Delta f N_s T_s\right)\cos\left(2\pi\Delta\theta N_s T_s\right)}\\
&=\cos\left(2\pi\Delta f N_s T_s\right)\cos\left(2\pi\Delta\theta N_s T_s\right)\\
&-\cos\left(2\pi\Delta f N_s T_s\right)\sin\left(2\pi\Delta\theta N_s T_s\right)\times\tan\left(2\pi\Delta\theta N_s T_s\right)\\
&=z_1
\end{aligned} \tag{2.2.8}$$

Since the sample time is 50 ns and the P-CFO us set to 30 ppm, $2\pi\Delta\theta N_s T_s$ is small and approximated as $\tan\left(2\pi\Delta\theta N_s T_s\right)$. Accordingly, the following equation holds:

$$\tan\left(2\pi\Delta\theta N_s T_s\right)\cong\sin\left(2\pi\Delta\theta N_s T_s\right)\cong 0 \tag{2.2.9}$$

So, z_1 can be approximated as

$$z_1\cong\cos\left(2\pi\left(\Delta f+\Delta\theta\right)N_s T_s\right) \tag{2.2.10}$$

Consequently, the frequency offset can be computed from (2.2.10).

$$\Delta\hat{f}=\frac{\cos^{-1}\left(z_1\right)}{2\pi N_s T_s}-\Delta\theta \tag{2.2.11}$$

The same method also indicates that

$$\begin{aligned}
&\frac{\mathrm{Im}\{R_3\}\mathrm{Re}\{R_1\}-\mathrm{Im}\{R_1\}\mathrm{Re}\{R_3\}}{2\left(\mathrm{Im}\{R_3\}\mathrm{Re}\{R_2\}-\mathrm{Im}\{R_2\}\mathrm{Re}\{R_3\}\right)}\\
&=\frac{\sin\left(4\pi\Delta f N_s T_s\right)\cos\left(4\pi\Delta\theta N_s T_s\right)}{2\sin\left(2\pi\Delta f N_s T_s\right)\cos\left(2\pi\Delta\theta N_s T_s\right)}\\
&=\cos\left(2\pi\Delta f N_s T_s\right)\cos\left(2\pi\Delta\theta N_s T_s\right)\\
&-\cos\left(2\pi\Delta f N_s T_s\right)\sin\left(2\pi\Delta\theta N_s T_s\right)\times\tan\left(2\pi\Delta\theta N_s T_s\right)\\
&=z_2\\
&\cong\cos\left(2\pi\left(\Delta f+\Delta\theta\right)N_s T_s\right)
\end{aligned} \tag{2.2.12}$$

From (2.2.12), the estimated frequency offset can be expressed as

$$\Delta\hat{f}=\frac{\cos^{-1}\left(z_2\right)}{2\pi N_s T_s}-\Delta\theta \tag{2.2.13}$$

Therefore, the estimated frequency offset can be averaged according to (2.2.11) and (2.2.13).

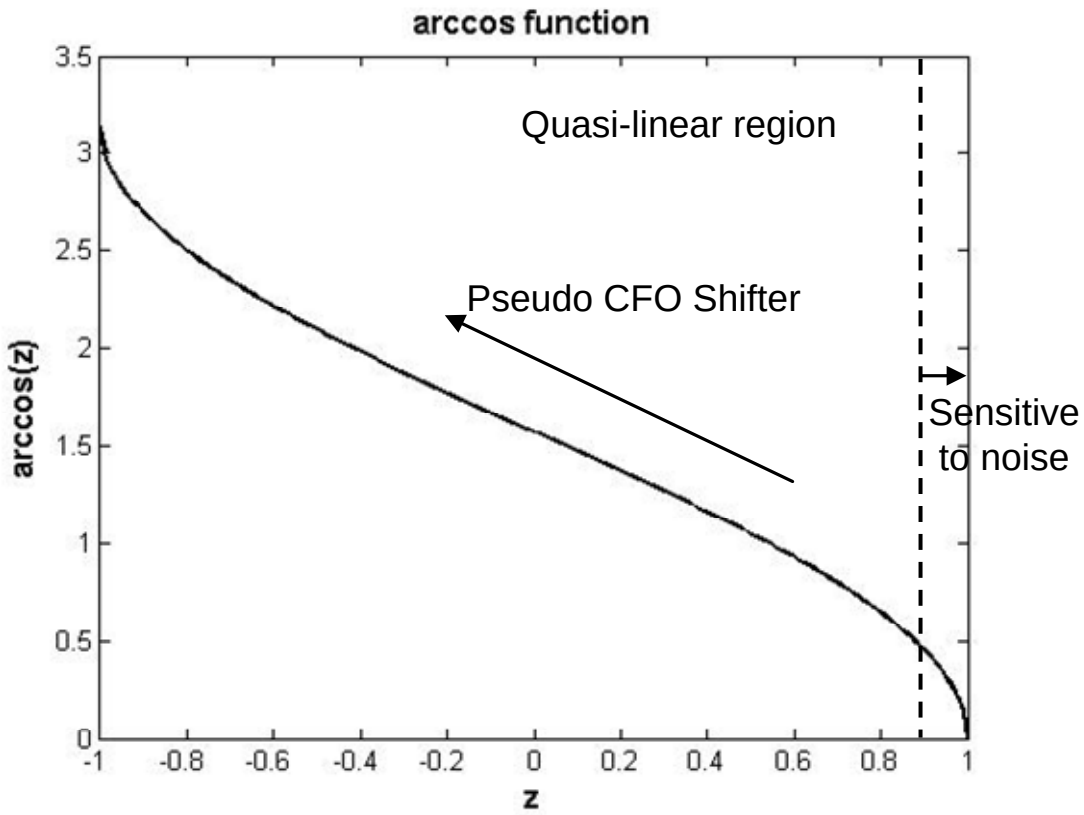

Figure 2-5 Inverse cosine function

Figure 2-5 shows the inverse cosine (arccosine) function for real element of z in the domain [-1, 1]. This figure indicates that the arccosine value should be zero if the original CFO value is 0ppm. However, there is a disadvantage of the cosine estimator ($\cos^{-1}(z)$). It is sensitive to even a small amount of noise disturbance when z is relatively small. Therefore, the noise disturbance will have great effect on the CFO estimation and lead to transformation errors. The proposed method to solve this problem is to multiply the training sequence by an extra exponential term and get a larger CFO value. A larger CFO value prevents inverse cosine from being affected by noise disturbance and reduces the possibility of transformation errors accordingly.

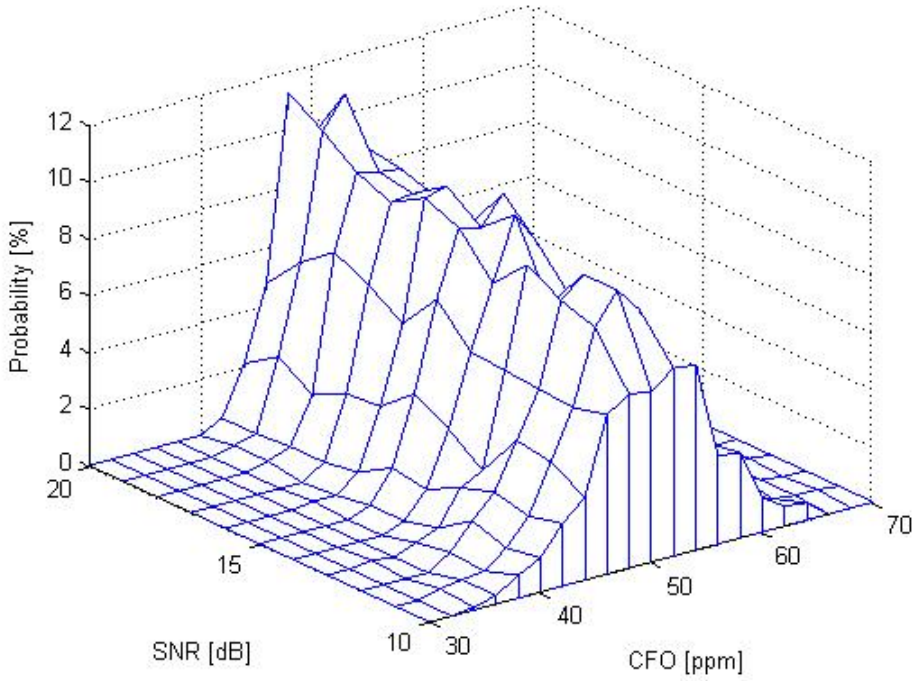

(a)

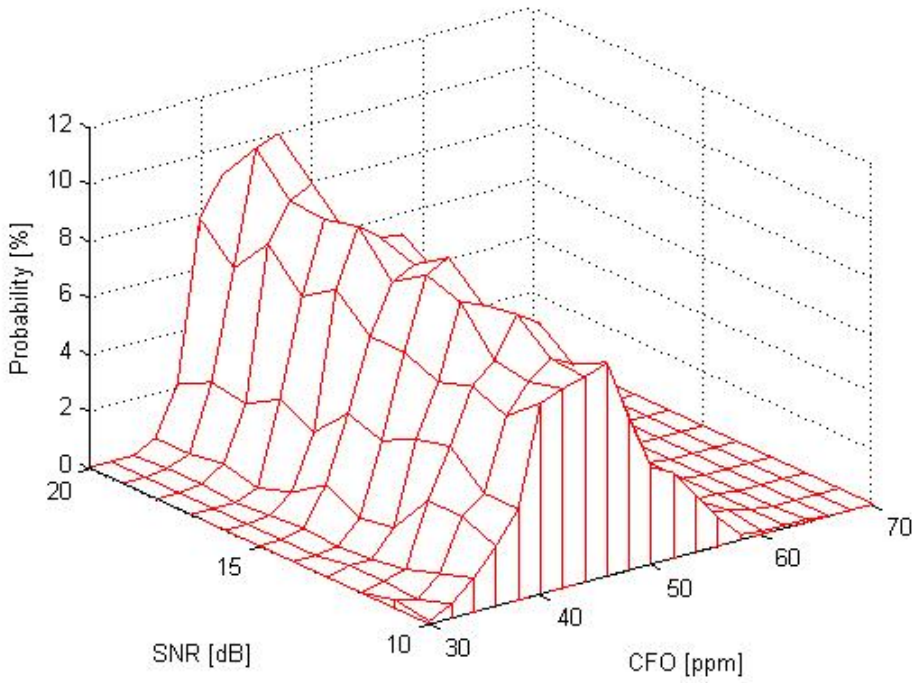

(b)

Figure2-6 PDF of 50 ppm: (a)FD-CFO algorithm (b)Moose's algorithm

The estimated frequency offset under IQ-M can be characterized by a Gaussian

probability density function (PDF), as shown in Figure 2-6(a) and (b). Figure 2-6(a) clearly shows that the mean of the proposed FD-CFO algorithm was close that of the original CFO. However, the Moose's algorithm, as shown in Figure 2-6(b), always had bias. These figures indicate that the proposed FD-CFO algorithm allows the correct CFO to be extracted under IQ-M conditions. Figure 2-7 shows the mean square error (MSE) of frequency estimation versus signal-to-noise ratio (SNR) under different IQ-M conditions. Figure 2-7 indicates that for almost the entire SNR range, the FD-CFO algorithm under the condition of 2-dB gain error and 20 phase error performed better than Moose's and Stefaan's algorithm [16], under the same condition or moderate IQ-M scenario, i.e., 1dB gain error and 10 phase error. The FD-CFO algorithm thus has better estimation accuracy under IQ-M than Moose's and Stefaan's algorithm. Since there are some approximations in the derivation, the MSE of the FD-CFO algorithm is slightly weaker than the Moose's algorithm under ideal I/Q. Although Stefaan's algorithm is constructed by a simple algebraic deduction and the estimation is independent of the IQ-M. That means the estimation results will not have variations no matter how severe the IQ-M is. As shown in Figure 2-7, the Stefaan's MSE lines overlap in the upper of the figure. Unfortunately, the Stefaan's algorithm is sensitive to the noise. So, the estimation error is much worse than FD-CFO under AWGN. TABLE 2-1 summarizes the required SNR when the MSE is on the order of 10-6.

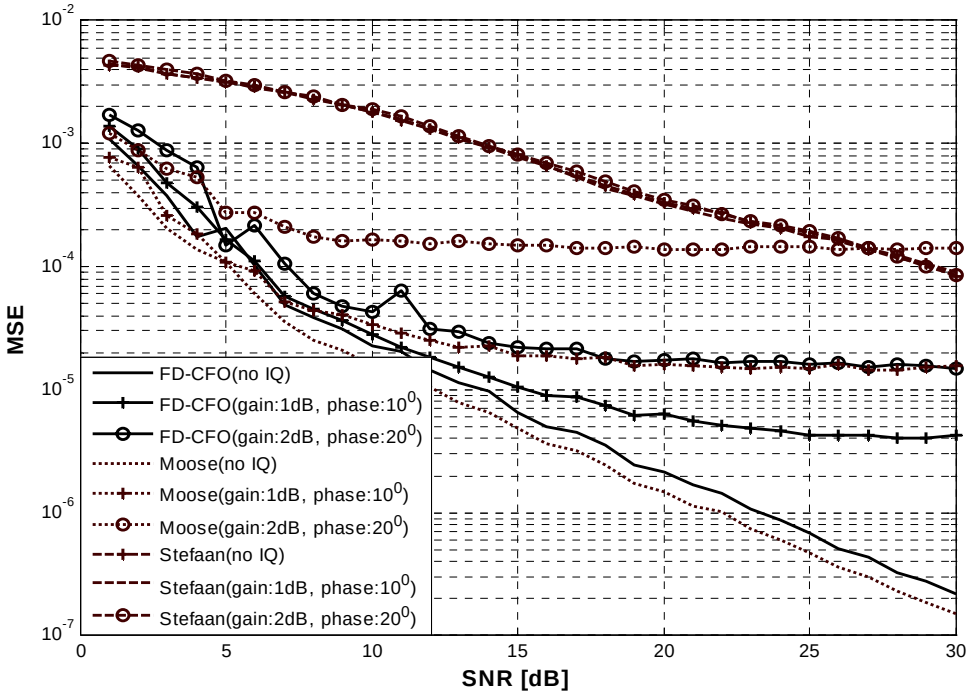

Figure 2-7 Mean square error (MSE) of frequency estimation versus SNR under different IQ-M with 50 ppm CFO

TABLE 2-1 REQUIRED SNR FOR 10^{-4} MSE

IQ-M	*Required SNR [dB]*		
	FD-CFO	Moose	Stefaan
No IQ	7	6	30
Gain: 1 dB, phase: 10-degree	7	6	30
Gain: 2 dB, phase: 20-degree	8	>30	30

Chapter 3

FD-BD Implementation

After a new short preamble point arrives and then be pushed into the FFT window to acquire the frequency response of short preamble. The frequency response will be multiplied with multiple patterns in restricted time. In order to catch up with the transmitted rate, multiple correlation banks are required. But the correlation bank cost too high to use excessively. So, that is trade-off between cost and performance. The compromising method is to use two correlation banks simultaneously and raise the system clock to 80 MHz. Therefore, the implementation can be done.

The input/output port definition of FD-BD is showed in Figure 3-1.FD-BD will take the frequency response of short preamble as the inputs and its outputs will be the estimated offset when complete the boundary detection.

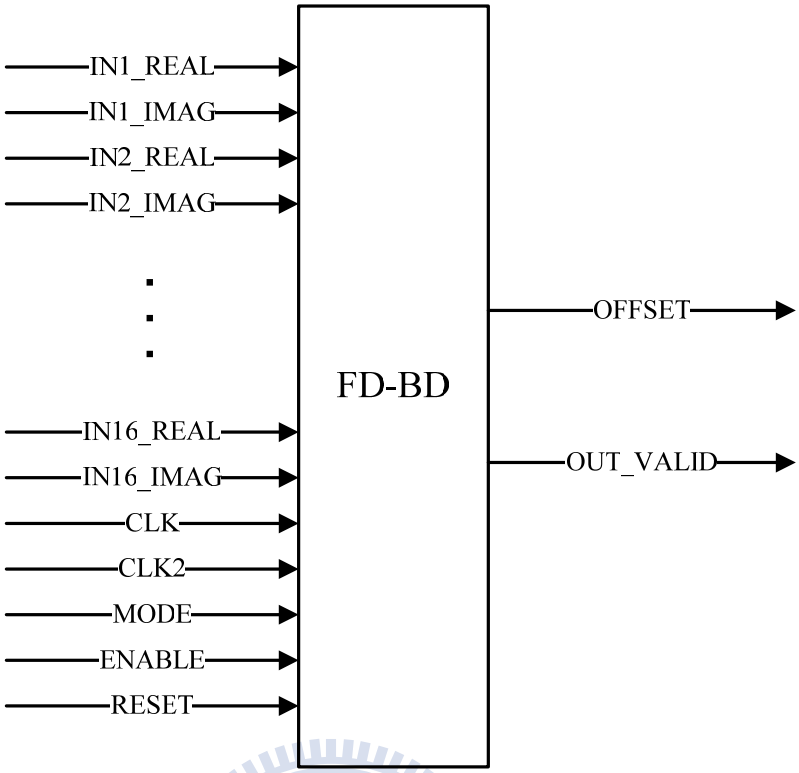

Figure 3-1 Input/output port definition of FD-BD

Figure 3-2 illustrates the VLSI architecture of the FD-BD algorithm, where the FD-BD scheme includes four main parts: FFT data buffer, Metric computation, Sorter and Interactive sequence searcher. There are two colours in the figure. The darker grey represents that operates at higher clock rate (77 MHz for DSSS or 80 MHz for OFDM). The lighter one operates at system clock rate (11 MHz for DSSS or 20 MHz for OFDM). When the frequency responses of training symbols are arrived, the Metric computation module is awakened to work. The task of Metric computation module is to compute the cross-correlation values between received training symbols and pre-stored frequency response of training symbol and its shift. In Figure 3-2, 4 ROMs are the role of lookup table to provide inputs of cross-correlations. When the computation is finished by the Metric computation module, Sorter module starts to sort the value of cross-correlation. As shown in Figure 3-2, inserter insert 2 values to sorted buffer each time until complete the sorting. After Sorter, the sorted values are sent to Interactive sequence searcher module. The task of Interactive sequence searcher module is to store candidates from sorted buffer and pass the candidates to

Memory module. Then, finger out where the symbol boundary is by Trellis rule checker module. Finally, the most frequency offset is the final boundary offset. The synthesis result of FD-BD is listed in TABLE 3-1 and the system clock rates are 11MHz for DSSS and 20MHz for OFDM in 0.18μm 1P6M CMOS, respectively. Summary is listed in TABLE 3-2. System parameters are listed in TABLE 3-3.

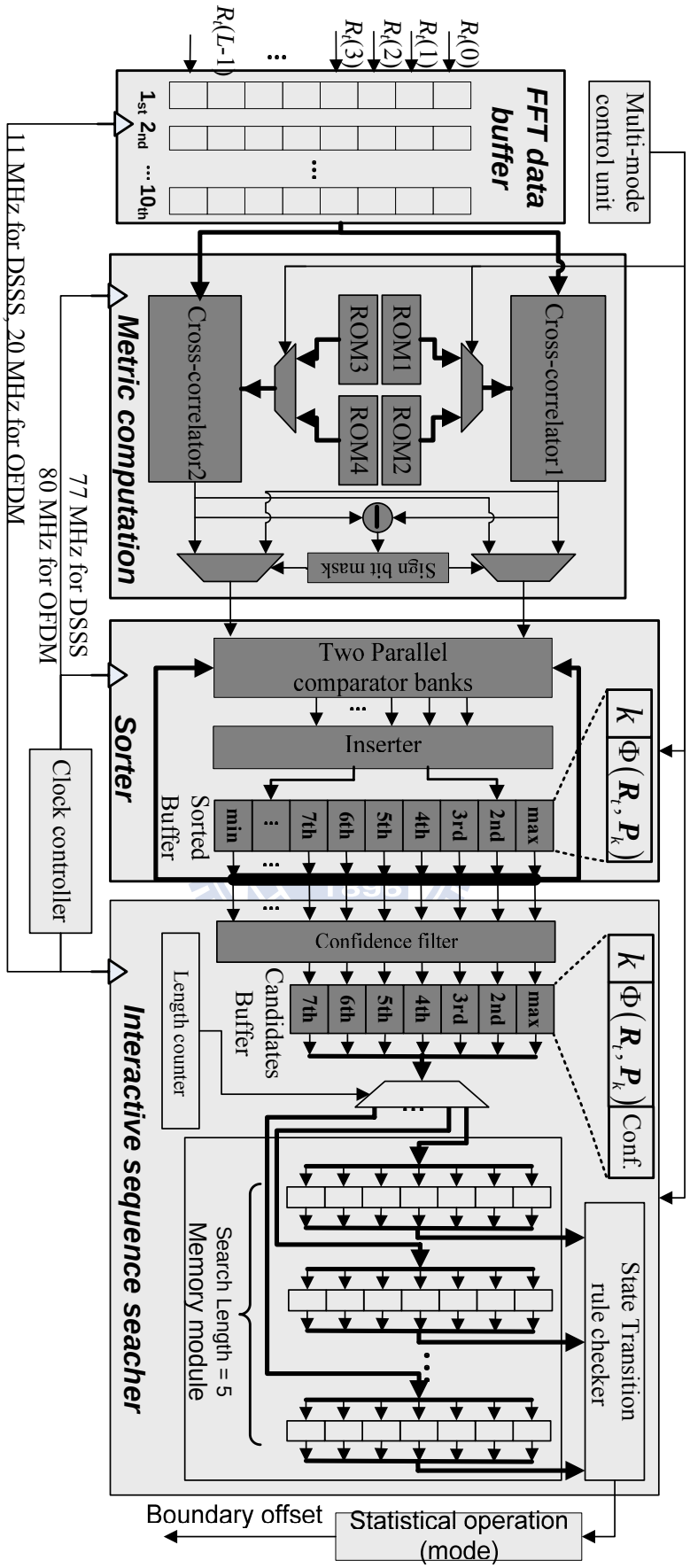

Figure 3-2 VLSI architecture of FD-BD

TABLE 3-1 SYNTHESIS RESULT OF FD-BD

Module	Gates	Percentage
Cross-correlation	230587	90.0%
Sorter	20631	8.1%
Iterative Sequence Search	4729	1.8%
Other(Control Units & Buffers)	130	0.1%
Total	256078	100%

TABLE 3-2 SUMMARY OF FD-BD

Technology	0.18-μm 1P6M CMOS
Gate Count	256 K
System Clock	80 MHz
Core Power	40.2 mW

TABLE 3-3 SYSTEM PARAMETER

Parameters	Value		
	DSSS	SISO-OFDM	MIMO-OFDM
Preamble type (# of chips)	±barker code (11 chips)	Short preamble (16 chips)	Short preamble (16 chips)
Chipping rate	11 MHz	20 MHz	20 MHz
FFT (used in sync. stage)	16	16	16

Chapter 4

FD-CFO Implementation

Figure 4-1 shows the input/output port definition of FD-CFO. FD-CFO will take the frequency response of short preamble as the inputs and its outputs will be the estimated CFO when complete the CFO estimation.

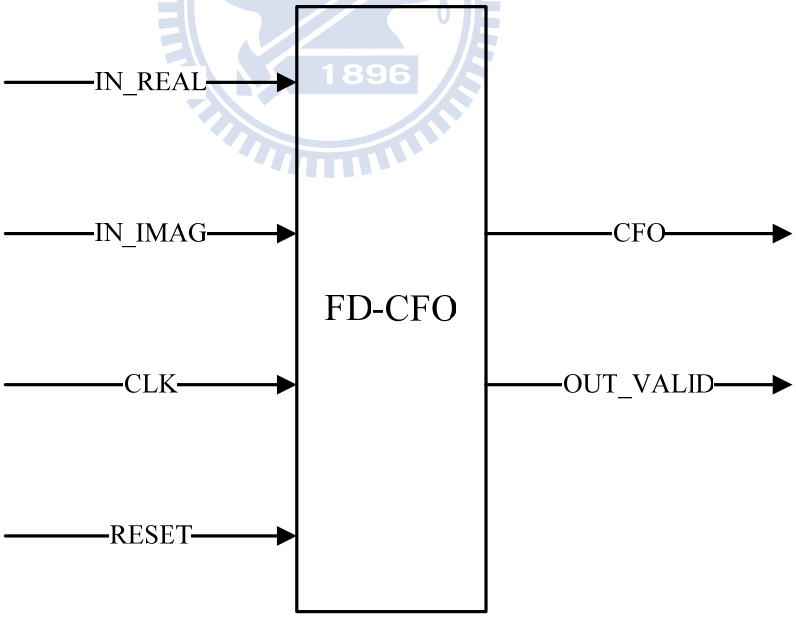

Figure 4-1 Input/output port definition of FD-CFO

Figure 4-2 is the VLSI architecture of FD-CFO. The FD-CFO contains three main parts: P-CFO shifter, CFO calculation and inverse cosine. The P-CFO shifter module begins to operate when the frequency responses of training symbols are arrival. The P-CFO shifter

module rotates the received frequency response of short preambles by the pseudo-frequency offset. As shown in Figure 4-2, the rotation is achieved by a look-up table and a complex multiplier. After the rotation is finished by the P-CFO shifter module, CFO calculation module begins to do estimation based on the FD-CFO algorithm. When the estimation of CFO is completed, the CFO calculation module sent its output to inverse cosine module. The assignment of inverse cosine module is to find the angle of the correction calculated from CFO calculation module, and then add/minus the pseudo frequency offset to extract the final CFO. The FD-BD is implemented via 0.18-μm CMOS library, which occupies approximately 49K gate count. The synthesis result of FD-CFO and summary of FD-CFP are listed in TABLE 4-1 and TABLE 4-2, respectively.

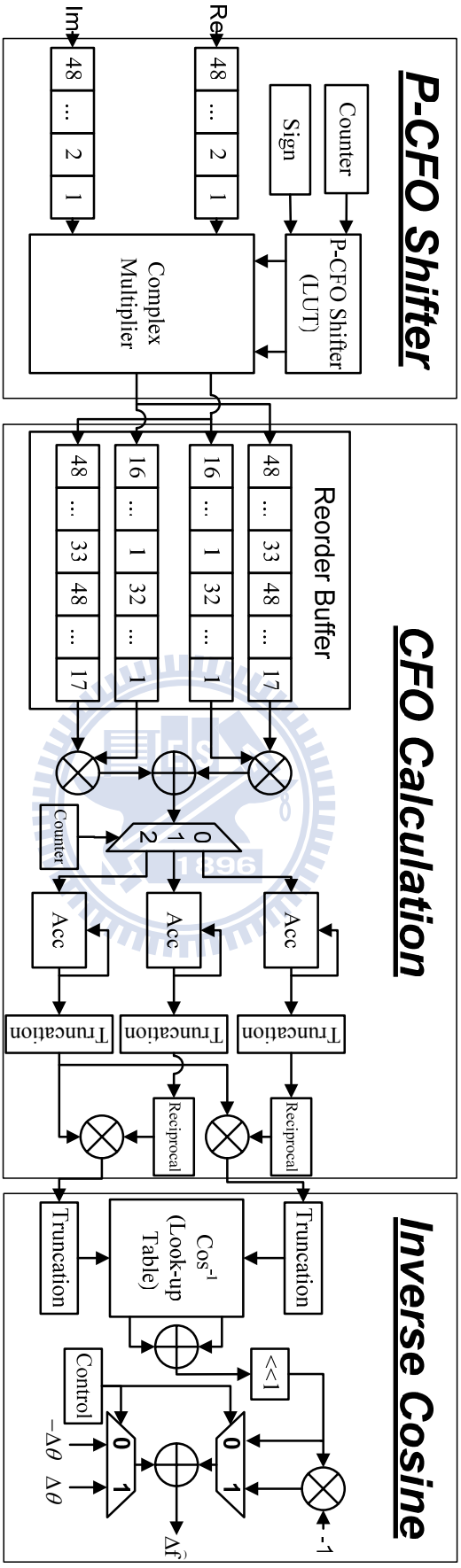

Figure 4-2 VLSI architecture of FD-CFO

TABLE 4-1 SYNTHESIS RESULT OF FD-CFO

Combinational area	298984.000000
Noncombinational area	146828.937500
Total cell area	445800.812500

TABLE 4-2 SUMMARY OF FD-CFO

Technology	0.18-μm 1P6M CMOS
Gate count	49 K
System clock	20 MHz

Chapter 5

Conclusion and Future Work

5.1 Conclusion

This work implements two synchronization algorithms in FD. The FD-BD adopts the MLSE-based iterative sequence search to find the offset in the symbols. Simulations results indicate the error rate is less than 1% in low-SNR environments. The results also hint that the SNR loss does not increase significantly even with the CFO is up to 100 ppm. Consequently, the FD-BD supporting DSSS and OFDM modes is implemented using an 0.18-μm 1P6M CMOS library. Although requires two correlation banks to keep up with the transmitted rate. However, the correlation function is often used in the synchronizer. After the operation of FD-BD, the correlation banks can be reused by other modules.

In addition, this thesis implements the FD-CFO which transfer the operation based on P-CFO from TD to FD. The performance of FD-CFO is comparable with P-CFO under I/Q mismatch. The FD-CFO can adopt three training symbols to estimate the frequency offset from -50 ppm to 50 ppm under 2.4 GHz carrier frequency with 2dB gain error and 20-degree phase error in multipath environments. Simulation results indicate that the average estimation error of the proposed FD-CFO algorithm can fulfil many system requirements, preventing obvious performance loss under different I/Q mismatch conditions.

5.2 Future Work

In IEEE802.11n, the standard is formulated the cyclic shift format of the short preambles in different antennas that are used to prevent unintentional beam-forming when the same signal or scalar multiples of one signal are transmitted through different spatial; streams or transmit chains. Cyclic shift means that every antenna transfers short preambles with different displacements contrast with original short preamble. Unfortunately, the cyclic shift will cause the correlation value of adjacent training symbols decreasing and then degrade FD-CFO performance. Simulation results show that there is 2dB degradation at least.

Furthermore, the continuous wave jamming (CW jamming) which is a kind of narrow band interference (NBI) can severely drop the performance of proposed algorithm and destroy the transmitted signal.

So some extensions to the research presented in this thesis will be included in out future work. In the future, the work is to improve the performance at low-SNR environments. The performance of FD-CFO should be ensured that will not be degraded under cyclic shift. Finally, increase the ability of resistance under CW jamming.

Bibliography

[1] R. V. Nee and R. Parsed, *OFDM for Wireless Multimedia Communication*. Natick, MA: Artech House, 2000.

[2] J. Heiskala and J. Terry, *OFDM Wireless LANs: A Theoretical and Practical Guide*. Indianapolis, IN: Sams, 2001.

[3] *Wireless LAN Medium Access Control (MAC) and Physical Layer (PHY) Specifications* , 1999, IEEE Std 802.11a.

[4] *Wireless LAN Medium Access Control (MAC) and Physical Layer (PHY) Specifications*, 2003, IEEE Std 802.11g.

[5] *Radio Broadcasting Systems: Digital Audio Broadcasting to Mobile, Portable and Fixed Receivers*, ETSI standard 300 401, Feb. 1, 1995.

[6] *Digital Video Broadcasting: Framing Structure, Channel Coding, and Modulation for Digital Terrestrial Television*, ETSI standard 300 421, Aug. 1, 1997.

[7] S. Y. Cheng and T. Y. Hsu, Frequency-Domain Frame Synchronization Using Iterative Sequence Search in Low-SNR Fading Environments.

[8] S. Hoyos, B. M. Sadler, and G. R. Arce, "Broad-band multicarrier communications receiver based on analog to digital conversion in the frequency domain," *IEEE Trans. Wireless Commun*., vol. 5, no. 3, pp. 652–661, Mar. 2006.

[9] P. K. Prakasam, M. Kulkarni, Xi Chen, Yu Zhuizhuan, S. Hoyos, J. Silva-Martinez, and E. Sanchez-Sinencio, "Applications of multipath transform-domain charge-sampling wide-band receivers," *IEEE Trans. Circuits Syst. II*, vol.55, no.4, pp.309-313, Apr. 2008.

[10] M. Lehne and S. Raman, "A prototype analog/mixed-signal fast fourier transform processor IC for OFDM receivers," *Proc. of IEEE Radio and Wireless Symposium 2008*, vol., no., pp.803-806, 22-24 Jan. 2008.

[11] F. Wang and Z. Tian, "Wideband receiver design in the presence of strong narrowband interference," *IEEE Commun. Lett*., vol.12, no.7, pp.484-486, July 2008.

[12] C. Panazio, "A frequency domain approach for non-coherent timing chip-level synchronization for cdma systems," *Proc. Of IEEE SPAWC 2007*, vol., no., pp.1-5,

17-20 Jun. 2007.

[13] W. H. Sheen and G. Stuber, "MLSE equalization and decoding for multipath-fading channels," *IEEE Trans. Commun.*, vol. 39, pp. 1455-1464, Oct. 1991.

[14] M. F. Sun, J. Y. Yu, T. Y. Hsu, Estimation of Carrier Frequency Offset With I/Q Mismatch Using Pseudo-Offset Injection in OFDM Systems, *IEEE Trans. On Circuits and Systems, vol. 55*, no. 3 Apr. 2008.

[15] P. H. Moose, "A technique for orthogonal frequency division multiplexing frequency offset correction," *IEEE Trans. Commun., vol. 42*, no. 10, pp. 2908–2914, Oct. 1994.

[16] S. dde Rore, "Joint estimation of carrier frequency offset and IQ imbalance for 4G mobile wireless systems," in *Proc. IEEE Int. Conf. Communications (ICC'06)*, Istanbul, Turkey, Jun. 2006, pp. 2066–2071.

[17] T. Pollet, M. van Bladel, and M. Moeneclaey, "BER sensitivity of OFDM systems to carrier frequency offset and wiener phase noise," *IEEE Trans Commun., vol. 43*, pp.191-193, Apr. 1993.